Since January 2020 Elsevier has created a COVID-19 resource centre with free information in English and Mandarin on the novel coronavirus COVID-19. The COVID-19 resource centre is hosted on Elsevier Connect, the company's public news and information website.

Virology 485 (2015) 422–430

Contents lists available at ScienceDirect

Virology

journal homepage: www.elsevier.com/locate/yviro

Intratracheal exposure of common marmosets to MERS-CoV Jordan-n3/2012 or MERS-CoV EMC/2012 isolates does not result in lethal disease

Reed F. Johnson [a,*], Laura E. Via [b], Mia R. Kumar [a], Joseph P. Cornish [a], Srikanth Yellayi [c], Louis Huzella [c], Elena Postnikova [c], Nicholas Oberlander [c], Christopher Bartos [c], Britini L. Ork [c], Steven Mazur [c], Cindy Allan [c], Michael R. Holbrook [c], Jeffrey Solomon [d], Joshua C. Johnson [c], James Pickel [e], Lisa E. Hensley [c], Peter B. Jahrling [a,c]

[a] Emerging Viral Pathogens Section, National Institute of Allergy and Infectious Diseases, National Institutes of Health, Frederick, MD, United States
[b] Tuberculosis Research Section, Laboratory of Clinical Infectious Diseases, National Institute of Allergy and Infectious Diseases, National Institutes of Health, Bethesda, MD, United States
[c] Integrated Research Facility, National Institute of Allergy and Infectious Diseases, National Institutes of Health, Frederick, MD, United States
[d] Center for Infectious Disease Imaging, Radiology and Imaging Sciences, Clinical Center, National Institutes of Health, Bethesda, MD, United States
[e] Transgenic Core Facility, National Institute of Mental Health, National Institutes of Health, Bethesda, MD, United States

ARTICLE INFO

Article history:
Received 2 April 2015
Returned to author for revisions
11 July 2015
Accepted 13 July 2015
Available online 3 September 2015

Keywords:
MERS
Middle East Respiratory Syndrome
MERS-CoV
Nonhuman primate
Animal model
Coronavirus

ABSTRACT

Middle East Respiratory Syndrome Coronavirus (MERS-CoV) continues to be a threat to human health in the Middle East. Development of countermeasures is ongoing; however, an animal model that faithfully recapitulates human disease has yet to be defined. A recent study indicated that inoculation of common marmosets resulted in inconsistent lethality. Based on these data we sought to compare two isolates of MERS-CoV. We followed disease progression in common marmosets after intratracheal exposure with: MERS-CoV-EMC/2012, MERS-CoV-Jordan-n3/2012, media, or inactivated virus. Our data suggest that common marmosets developed a mild to moderate non-lethal respiratory disease, which was quantifiable by computed tomography (CT), with limited other clinical signs. Based on CT data, clinical data, and virological data, MERS-CoV inoculation of common marmosets results in mild to moderate clinical signs of disease that are likely due to manipulations of the marmoset rather than as a result of robust viral replication.

Published by Elsevier Inc.

Introduction

Infection with Middle East Respiratory Syndrome Coronavirus (MERS-CoV) has been associated with Middle East Respiratory Syndrome commonly known as MERS, a respiratory syndrome with acute severe hypoxic respiratory failure often accompanied by renal failure (Arabi et al., 2014; Assiri et al., 2013; Zaki et al., 2012). As of March, 2015 there have been approximately 1000 laboratory confirmed cases reported with a 36% case fatality rate (http://www.who.int/csr/disease/coronavirus_infections/). Considering the geographical location of MERS and the Hajj pilgrimage which draws an estimated 2.5 million visitors, roughly 1.8 million of whom travel internationally (http://www.cdsi.gov.sa/english/index.php?option=com_docman&Itemid=173) MERS-CoV represents a global health risk. Common signs and symptoms of MERS include fever, cough, shortness of breath, and myalgia. Gastrointestinal signs are also frequently observed which include vomiting, diarrhea, and abdominal pain (Assiri et al., 2013). Often, MERS patients also have underlying comorbidities such as diabetes, hypertension, and chronic cardiac or renal disease (Assiri et al., 2013).

To guide development of MERS countermeasures, an appropriate animal model must be identified and characterized. Ideally, a laboratory animal model would demonstrate clinical signs consistent with all aspects of human disease. As with most infectious diseases, mice have been evaluated as a potential MERS model for pathogenesis and countermeasure screening. Balb/c and STAT-1 knockout mice did not develop signs of disease, such as weight loss, nor could infectious virus be recovered from lung homogenates (Coleman et al., 2014). Zhao et al. developed a murine model for MERS by transduction of the respiratory tract with the putative MERS-CoV receptor, human dipeptidyl peptidase 4 (DPP4 or CD26), using an adenovirus construct (Zhao et al., 2014). Infected mice developed limited clinical signs including a

* Corresponding author. Fax: +1 301 631 7389.
E-mail address: johnsonreed@mail.nih.gov (R.F. Johnson).

http://dx.doi.org/10.1016/j.virol.2015.07.013
0042-6822/Published by Elsevier Inc.

small degree of weight loss. Histopathological analysis found peribronchial and perivascular lymphoid infiltrates which later progressed to an interstitial pneumonia. Nearly 6 $\log_{10}$ plaque forming units (PFU)/g of infectious virus could be detected in the lungs of infected DPP4 transduced mice (Zhao et al., 2014). The DPP4 transduced mouse model has been used to evaluate countermeasures and pathogenesis (Channappanavar et al., 2014a, 2014b).

Nonhuman primate (NHP) models are considered to be essential to understanding pathogenesis and evaluating countermeasures. Results from several challenge studies of MERS-CoV in rhesus monkeys (*Macaca Mulatta*) have varied between laboratories. The first published NHP model used rhesus monkeys inoculated via multiple routes and evaluated for virological, immunological, and histopathological changes up to 6 days post-inoculation (de Wit et al., 2013). NHPs demonstrated signs of pneumonia and virus could be detected in tissues and mucous membranes by quantitative reverse transcriptase polymerase chain reaction (qRT-PCR), but attempts to determine the load of infectious virus was not reported. A follow up study demonstrated that administration of interferon-alpha2b and ribavirin reduced viral burden and lessened disease (Falzarano et al., 2013). Results from a natural history study of MERS-CoV-infected rhesus monkeys indicated that intratracheal inoculation induced a non-lethal disease with limited pathology observed in recovering animals at 28 days post-inoculation and infectious virus could be recovered from lung but not other tissues assayed (Yao et al., 2014). Standard radiological examination revealed lung infiltrates at days 3 and 5 post-inoculation, suggesting virus-induced lung disease. More recently, Falzarano et al. described multiple route inoculation of the common marmoset (*Callithrix jacchus*) in which transcriptional changes indicating induction of immune, inflammatory, and repair pathways were cataloged and partial lethality was observed (Falzarano et al., 2014).

Here we characterize intratracheal (IT) inoculation of MERS-CoV into common marmosets as a model for MERS and to determine differences between two common isolates of MERS-CoV, MERS-CoV-Jordan-n3/2012 virus and MERS-CoV-EMC/2012 virus. We inoculated 4 groups of marmosets and followed disease progression by periodic physical exams that included computed tomography (CT). Previously, positron emission tomography with computed tomography (PET)/CT has been used to evaluate tuberculosis therapies in common marmosets (Via et al., 2013), disease progression in monkeypox-virus-inoculated cynomolgus monkeys (Dyall et al., 2011), and influenza-A-virus-inoculated ferrets (Jonsson et al., 2012). CT has two distinct advantages when compared to standard x-ray radiography 1) CT provides three dimensional data, and 2) CT data can be quantified, which allows unbiased comparisons (Elke et al., 2013; Li et al., 2013; Romanova et al., 2014).

Results

An ex-vivo experiment with marmoset lung and kidney primary cultures found that these tissues could support MERS-CoV replication; this suggested that common marmosets might be developed as a suitable animal model for MERS (Fig. 1). Therefore, we sought to determine if intratracheal inoculation of marmosets would result in disease presentation similar to human disease. The experimental design is shown in Fig. 2. Two pre-inoculation baseline CT's were performed to establish normal lung volumes and any pre-existing anomalies.

MERS-CoV-Jordan-n3/2012 virus (MERS-JOR, Genbank KC776174) and MERS-CoV-EMC/2012 virus (MERS-EMC, Genbank JX869059) were obtained and propagated as described in Materials and Methods. To ensure that no gross cross-contamination of

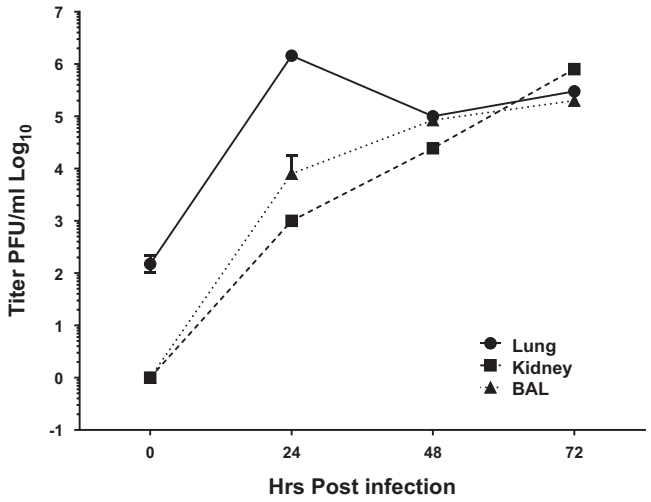

Fig. 1. Ex-vivo analysis of primary cells. Cells were isolated from lung, kidney, and bronchoalveolar lavage (BAL), and one-step growth kinetics were performed as described in Materials and Methods. Lung, Kidney and BAL demonstrate that MERS-CoV is able to replicate to at least 4 $\log_{10}$ PFU/mL.

the MERS-CoV stocks used for the marmoset experiments occurred during preparation, the spike protein of each stock was sequenced and compared to reference sequences (Cotten et al., 2013; Frey et al., 2014). The spike region was chosen for comparison due to high diversity associated with viral glycoproteins. Strain-specific differences found in MERS-JOR and MERS-EMC reference sequences were maintained in our stocks (Table 1), indicating that no gross cross-contamination occurred. Three single nucleotide polymorphisms (SNPs) were seen in our stocks, two in MERS-EMC and one in MERS-JOR. BLASTX alignments indicate that two of these SNPs lead to changes in the S2 protein sequence. The MERS-JOR stock had a T to C change at position 2636 which induced an I839T change in S2. Two changes were observed in MERS-EMC C to T at position 2604 that did not alter amino acid sequence and a C to A change at 3044 which resulted in a N1016T change in S2. Changes in the S2 region seen here are likely a result of serial passage in cell culture (Frey et al., 2014).

Clinical signs and hematology indicate mild disease

Body temperature, peripheral oxygen saturation, respiratory rate, and overall condition were evaluated at each physical exam. No increases in body temperatures above normal ranges were observed; subjects maintained peripheral oxygenation throughout the study, and respiratory rates increased above normal range sporadically throughout the study (Fig. 3A). Tremors were noted on daily observations including and between days 3 and 9 post-inoculation, but were not consistently observed (data not shown).

Subjects underwent blood withdrawal on days 0, 4 or 5, and at necropsy to determine if hematological parameters indicated changes consistent with disease. Day 4 or 5 was chosen based on our data from MERS-JOR inoculated rhesus monkeys which demonstrated a peak in lung disease at day 5 post-inoculation by CT (manuscript in preparation). Subjects did not develop clinically significant changes in total white blood cell count, lymphocyte number, monocyte number, or neutrophil number on day 4 or 5 post-inoculation and remained within the normal range, as indicated by shaded gray area (Fig. 3B). Together, these data indicate that subjects did not develop systemic clinical disease.

To determine if virus was disseminating or shedding, whole blood, oropharyngeal, rectal swabs, and fecal samples from mock and inactivated virus subjects, 2 subjects per group, were collected on days −21, −8, 1, 3, 5, 7, 14 or 15, and 25. MERS Jordan subjects

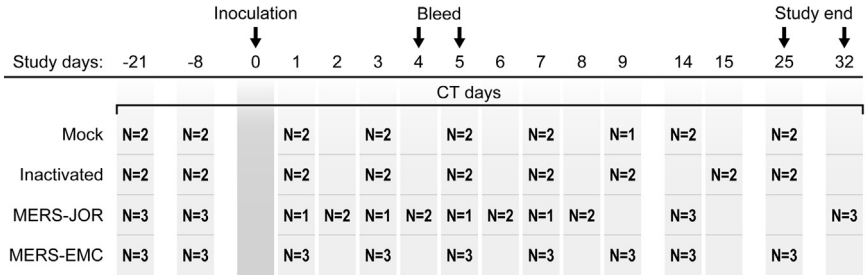

Fig. 2. Experimental study design. Four groups of common marmosets were inoculated with virus culture growth media (mock), 5×10^7 PFU of γ-irradiated (inactivated) MERS-JOR, or MERS-EMC, 5×10^7 PFU of MERS-JOR, or 5×10^7 PFU MERS-EMC. Procedures were performed when indicated.

Table 1
MERS-CoV Spike Sequence comparison.

Spike alignment position	MERS-JOR reference sequence (Genbank KC776174)	MERS-JOR study stock	MERS-EMC reference sequence (Genbank JX869059)	MERS-EMC study stock
281	G	G	U	U
580	C	C	U	I
902	G	G	U	U
2604	C	U	C	C
2636	U	U	U	C
3044	A	A	G	G
3249	C	C	G	G
3285	G	G	U	U
3472	U	U	C	C
3591	C	C	U	U
3669	C	C	U	U
3753	C	C	U	U
3792	C	C	U	U

were swabbed on days −21, −8, 1 ($n=1$), 2 ($n=2$), 3($n=1$), 4 ($n=2$), 5($n=1$), 6 ($n=2$), 7($n=1$), 8($n=2$) 14($n=3$) and 32 and MERS-EMC exposed subjects were swabbed on days −21($n=3$), -8 ($n=3$), 1($n=3$), 3 ($n=3$), 5($n=3$), 7($n=3$), 14($n=3$), and 25 ($n=3$) as outlined in Fig. 2. These samples were assayed by qRT-PCR as described in Materials and Methods. All samples were negative for MERS-CoV, suggesting that virus did not disseminate nor was shed. Furthermore, plaque assays were performed on necropsy tissues and no infectious virus could be detected. Virus isolation was attempted using lung homogenates for two sequential passages on Vero cells; no infectious virus could be detected.

Antibody response to MERS-CoV inoculation

Fluorescent reduction neutralizing assays were performed to determine if marmosets developed an antibody response to MERS-CoV (Fig. 4). Subjects inoculated with MERS-JOR developed a low antibody titer to MERS-CoV with an average titer of 1:100 across the group at study end, day 25–32 post-inoculation. Animals inoculated with MERS-EMC developed an antibody titer of 1:80 for all 3 subjects. Media only, and inactivated virus did not develop detectable neutralizing antibody responses to MERS-CoV.

CT suggests moderate lung disease

Qualitative assessment of the imaging data indicates that MERS-CoV inoculated marmosets developed lung disease that mainly affected the medial and caudal regions of the lung. Lung abnormalities could be observed in media-only and the inactivated virus inoculation groups, with the inactivated virus stimulating increased lung abnormalities when compared to the media only mock inoculated subjects (Fig. 5A). Lung infiltrates presenting as air bronchograms did not completely clear by end of study (Fig. 5B).

More importantly, quantitative assessment of abnormal lung volume data supported the qualitative assessment. The quantitative assessment suggests that mock inoculated subjects developed a short lived response that was observed one day post-inoculation but returned to near baseline by the day 7 CT and remained near that volume throughout the course of the study. Subjects inoculated with inactivated virus demonstrated increased abnormal lung volumes when compared to the media only group, but not as elevated as the groups that received live virus. MERS-CoV inoculated groups demonstrated increasingly abnormal lung volumes beginning day 1 post-inoculation in an individual dependent manner that did not completely resolve by study end (Fig. 5C and D). Comparison of the mean peak values of diseased lung volume and percent relative change of abnormal lung volume for each group indicated no statistically significant difference (unpaired t-test) between the virus isolates (Fig. 5E and F). When the peak diseased lung volume of the infectious MERS-EMC receiving group is compared to the mock infected the p-value$=0.026$ and when compared to the γ-irradiated virus receiving group it is $p=0.548$. Comparison of the MERS-JOR group to the control groups indicates a similar pattern $p=0.057$ and $p=0.1245$, respectively. Comparison of the % fold change in diseased lung volume between the MERS-EMC and mock group gave $p=0.0049$ and the γ-irradiated virus receiving group was 0.0195. Comparison of the % fold change in diseased lung volume between the MERS-JOR and mock group gave $p=0.2102$ and $p=0.1591$. The data indicate that, in common marmosets, the genetic sequence differences between the isolates do not impact disease progression as indicated by changes in diseased lung volume and that the MERS virion itself can induce an inflammatory response. However, a significant difference was observed between the MERS-EMC group and the mock exposed group when compared by fold change of diseased lung volume, which likely reflects the small group sizes. Differences in temporal progression were observed between the individual subjects that did not segregate by virus isolate.

One subject in the MERS-EMC inoculated group appeared to develop a secondary infection observed by CT that increased to study end, day 25 post-exposure. However, no infectious virus could be recovered, suggesting an opportunistic infection either due to repeated manipulations or effects of MERS-CoV.

Pathology supports CT findings

At necropsy, lung lesions included multifocal to coalescing interstitial pneumonia with consolidation of the dorsocaudal lung lobe in the MERS-CoV inoculated animals (Fig. 6). Gross pathology of MERS-CoV infected subjects revealed no to moderate changes. These changes include interstitial multifocal to coalescing moderate pneumonia as shown in Fig. 6A. Histopathological examination of select lymphoid tissues revealed mild lymphoid hyperplasia, with

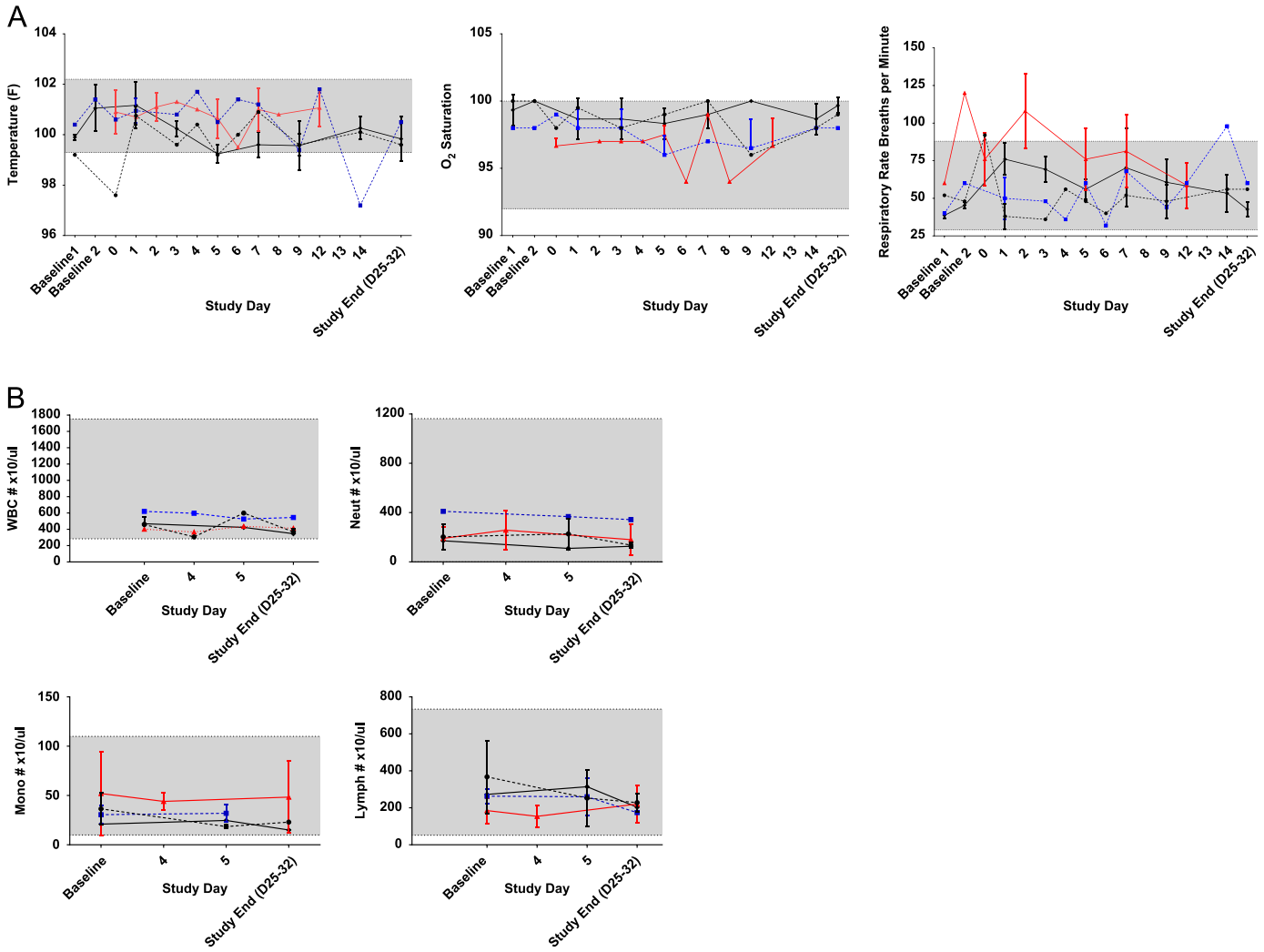

Fig. 3. Select clinical parameters through the course of the study. (A) Temperature and peripheral oxygen saturation are within normal values throughout the course of the study. Respiratory rate is elevated in virus-inoculated groups from day 3 to day 12 post-inoculation. (B) Clinical hematology suggests minimal-to-mild changes throughout the course of the experiment that remained within normal range (gray shaded area). Black-dashed line indicates mock-inoculated group, blue-dashed line indicates inactivated-virus-inoculated group, red line indicates MERS-JOR-inoculated group, and black line indicates MERS-EMC-inoculated group.

medullary histiocytosis of the mandibular and tracheobronchial lymph nodes in several of the MERS-CoV inoculated subjects, while the control animals showed minimal changes. Examination of representative lung tissue samples showed interstitial lymphohistiocytic pneumonia with type II pneumocyte and bronchial associated lymphoid tissue (BALT) hyperplasia and a few syncytia were observed in the MERS-CoV inoculated animals (Fig. 6B and D). In addition, the lung lesions observed in the MERS-CoV inoculated subjects are consistent with a chronic respiratory disease. In general, the gross and histopathological findings in the lung tissue did somewhat correspond with the CT findings. Examination of representative lung tissue from a single subject that received MERS-JOR and demonstrated the greatest increase in diseased lung volume as seen by CT did not differ grossly or histologically from the other subjects. No signal was detected for the presence of MERS-CoV antigen by immunohistochemistry (IHC) performed on the lung tissue sections of the infected subjects.

Discussion

Ideally, an animal model for MERS will recapitulate the key features of the human disease in the severe form. Therefore, an ideal MERS model might result in lethal disease with severe bronchopneumonia and extrapulmonary complications such as renal failure. With the use of CT, we observed that IT inoculation of common marmosets with MERS-JOR or MERS-EMC isolates resulted in a non-lethal disease characterized by limited clinical signs and moderate consolidative lung pathology that did not completely resolve by study end. No difference in clinical signs was observed between the two isolates or control subjects, nor could we detect MERS-CoV genome using a genome specific qRT-PCR assay with a sensitivity of 100 genome copies of MERS-CoV. Detection of neutralizing antibody in the infectious virus receiving groups and not the γ-irradiated virus receiving group does suggest that an infectious process did take place which allowed for antigen processing for development of neutralizing antibodies.

Artifacts introduced by manipulation of the subjects should be accounted for by use of control subjects. Control marmosets were inoculated with media or inactivated virus which also resulted in limited lung pathology. In the present study, examining the percent change in diseased lung volume determined a significant difference was observed between the MERS-EMC group and the mock group, but not between the MERS-EMC and γ-irradiated group, which suggests that some viral-induced disease process did occur. However, statistical significance was not found when the

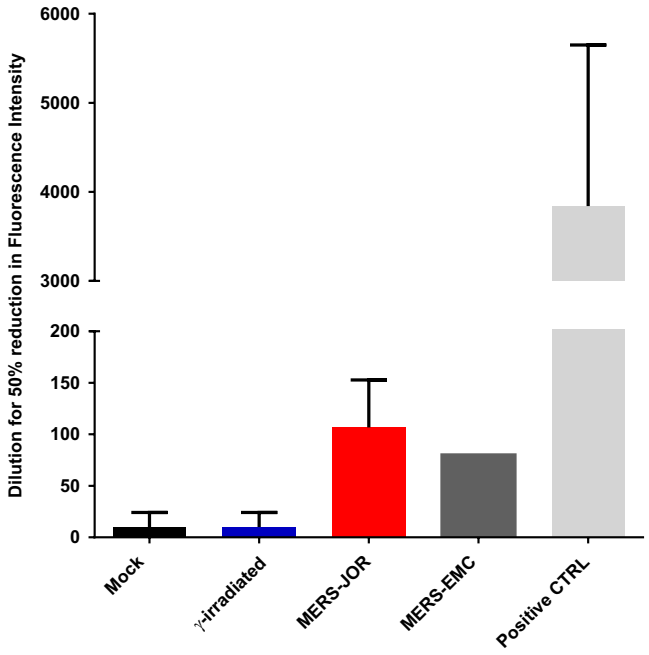

Fig. 4. Fluorescence Reduction Neutralizing Assay. Sera from all subjects was evaluated for the presence of neutralizing antibody to MERS-CoV as described in Materials and Methods. Neutralizing antibody could be detected above the background of the Mock infected subjects (1:10 $FRNA_{50}$ average) for subjects that received infectious MERS-CoV, γ-irradiated virus receiving subjects also develop background (1:10 $FRNA_{50}$ average) neutralizing antibody.

total diseased lung volumes were compared between any of the groups. Across all groups, pathology findings were predominantly confined to the lungs showing chronic and resolving changes. The absence of viral antigen signal in the lung tissue sections by IHC might be a result of probing for the viral antigen only at a late stage of disease, when there was likely considerable clearance of the virus.

Falzarano et al. observed inconsistent lethality highlighted by lung pathology that shared some characteristics of MERS following MERS-EMC exposure of common marmosets. Three notable differences between the present study and Falzarano et al. are 1) our use of control subjects receiving media or inactivated virus, 2) single IT route vs. multiple inoculation routes (oral, intranasal, ocular, and IT), and 3) the volume of lung inoculum (0.2 mL vs. 0.5 mL). Similar to their rhesus experiment, their marmoset experiment was designed as a serial euthanasia study. Six subjects were euthanized at early timepoints post-exposure, before the disease course could resolve. However, two subjects met moribund endpoint criteria on day 4, and 3 survived to day 20 post-inoculation. It is unknown what the true outcome of the subjects that were serially euthanized would have been and if the subjects that met endpoint criteria did so due to virus induced disease or subject manipulations, thus skewing the interpretation of disease severity. Adding to the difficulty in data interpretation, qRT-PCR data is not supported by immunohistochemistry, EM, or virus isolation. Furthermore, the pattern of infectious virus isolation shown by Falzarano et al. demonstrates that initially only the lungs contain infectious virus in 11/15 tissues (trachea and lung lobes) examined, by day 4 post-inoculation virus can be isolated from fewer lung lobes (8/10 tissues), but virus can be isolated from the trachea. By day 6 post-inoculation virus is detected in 1/8 of lung lobes and all tracheas examined. No quantification is provided, therefore it is difficult to determine if propagated infectious virus was recovered or merely the inoculum. Based on our data and Falzarano et al.'s data, it is possible that intratracheal inoculation results in mechanical damage to the respiratory epithelium, followed by inflammation and repair, which leads to restoration of mucociliary motion that clears the liquid (and virus) from the lung.

In the absence of a lethal model, other quantitative measures become more valuable for demonstrating pathogenesis. In the present study, we demonstrated that CT is effective for evaluating disease progression and regression following MERS CoV exposure in common marmosets. CT data can be quantified, which provides an opportunity to effectively evaluate countermeasures in sub-optimal models and strengthen data gained in well-established models. In the case of MERS, an optimal animal model must still be developed. Staged euthanasia studies similar to the adenovirus transduced mouse MERS model could be performed in NHPs, but such studies are undesirable due to the ethical concerns of nonhuman primate use.

Materials and methods

Virus and cells

Vero cells (ATCC catalog number CCL81) were maintained in Dulbecco's Modified Eagle's medium (DMEM) (HyClone, Logan, UT) and supplemented with 10% fetal bovine serum (FBS) (Sigma St. Louis MO) at 37 °C with 5% CO_2. MERS-CoV isolates (Jordan-n3/2012 and EMC/2012) were propagated at a multiplicity of infection of 0.1 on Vero cells in 5% FBS and 5% CO_2 for 3–4 days post-inoculation until cytopathic effect encompassed 75–80% of the Vero cell monolayer. Virus was concentrated by ultracentrifugation and pelleted through a 20% sucrose cushion at 221,000 × *g* for 2 h at 4 °C. The pellet was re-suspended in DMEM 5% FBS, frozen and titered by limiting dilution plaque assay (see below). Inactivated virus for the control groups was generated by treating virus with 60,000 Gy of gamma irradiation from a ^{60}Cobalt irradiator (JL Shepherd 484-R2), followed by confirmation of inactivation. MERS-CoV-Jordan-n3/2012 was a kind gift of Armed Forces Health Surveillance Center, Division of Global Emerging Infections Surveillance and Response System and MERS-CoV-EMC/2012 was kindly provided by Vincent Munster, Laboratory of Virology, National Institute of Allergy and Infectious Diseases (NIAID).

Tissue processing and growth curves in primary marmoset cells

Marmoset lung tissue was ground in a sterile petri dish using a plunger from a sterile syringe, digested with 100 U/ml of collagenase (Life Technologies, NY USA), and 10% fetal calf serum (FCS, HyClone) 37 °C for 30 min. The reaction was quenched, and the homogenate was passed through a 70-μm filter, washed, and centrifuged (500 × *g*, 5 min, 4 °C). After the final wash, cells were re-suspended in 5 ml of ACK Lysing Buffer (Life Technologies) for 15 min and washed twice with 25 ml PBS/5 mM EDTA/0.5% BSA. Washed and pelleted cells were re-suspended in RPMI (Lonza, Switzerland) supplemented with 10% FCS (HyClone, UT, USA) and 1% penicillin/streptomycin (PS) and plated. Media was changed after 24 h. Kidneys were processed similar to the lung but strained through 70 μm and 40 μm filters prior to the ACK lysis step. Bronchoalveolar lavage samples were centrifuged at 1000 × *g* for 10 min at 4 °C, re-suspended in RPMI 10% FCS, and 1% PS (Life Technologies) before plating. Multi-step growth curves were performed on isolated primary cells infected with MERS-JOR at a multiplicity of infection of 0.1. Supernatants were harvested at 0, 24, 48, and 72 h and stored at −80 °C until plaque assays were performed (described below).

Sequencing of MERS-CoV Spike protein and data analysis

MERS-CoV isolates were sequenced using the primers in Table 2. Spike genomic sequences were generated by aligning Sanger

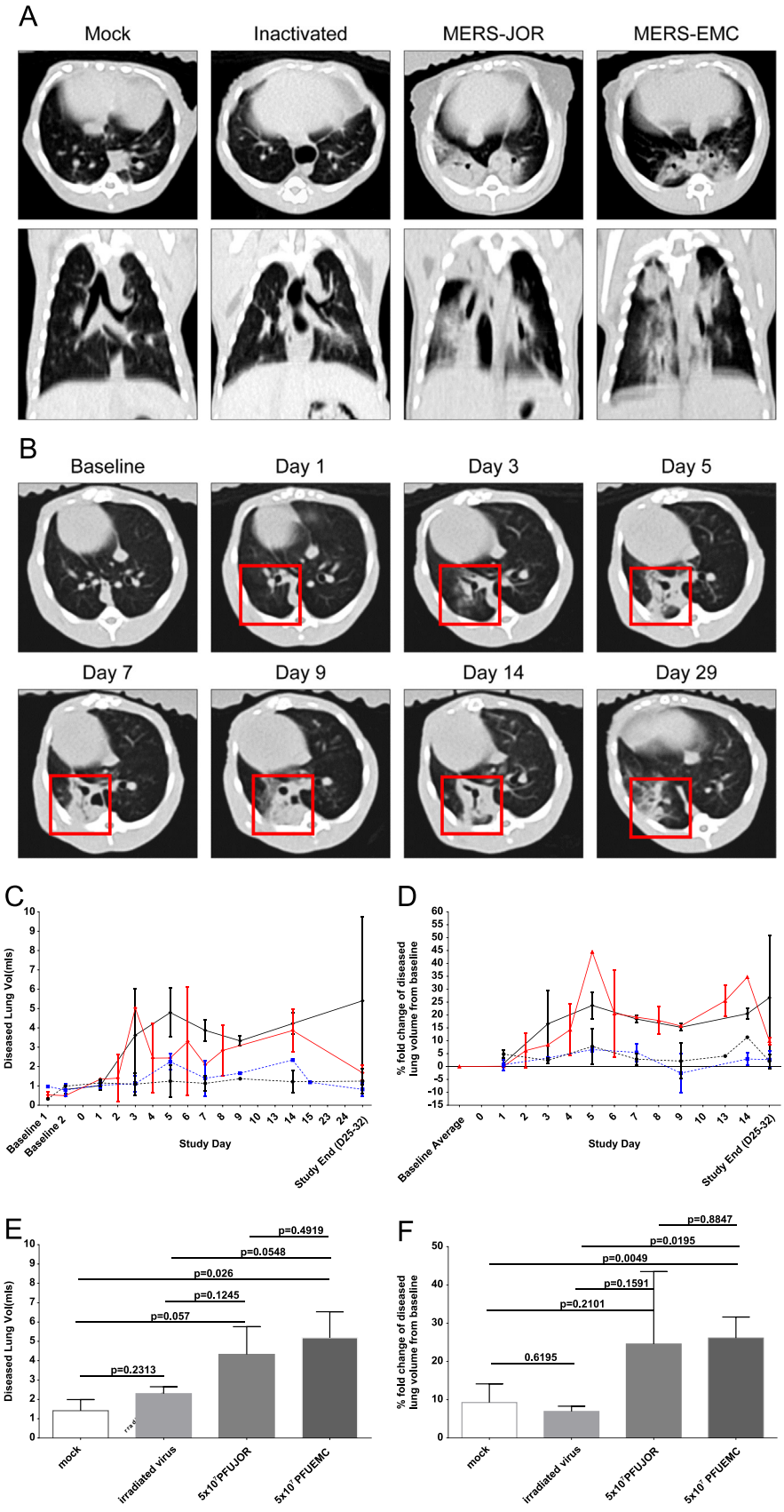

Fig. 5. Representative lung CT images demonstrating disease presentation. (A) Comparison of a representative subject from each of the 4 groups at 5 days post-inoculation. (B) Lung CT of representative subject that received the MERS-EMC isolate throughout the course of the study. Red boxes indicate regions of lung pathology that were first observed at day 3 post-inoculation and persisted to study end. (C) Quantification of total diseased lung volume. Black dashed line indicates mock-inoculated group, blue line indicates inactivated-virus-inoculated group, red line indicates MERS-JOR-inoculated group, and black dashed line indicates MERS-EMC-inoculated group. (D) Fold change from baseline of diseased lung volume. Black dashed line indicates mock inoculated group, blue line indicates inactivated virus inoculated group, red line indicates MERS-JOR inoculated group, and black dashed line indicates MERS-EMC inoculated group. (E) Comparison of the mean peak values to the media only instilled group on a total diseased volume basis. *t*-Tests were performed, $p \leq 0.05$ for significance. (F) Comparison of the mean peak values compared to the media only group as measured by fold change from baseline. *t*-Tests were performed, $p \leq 0.05$ for significance.

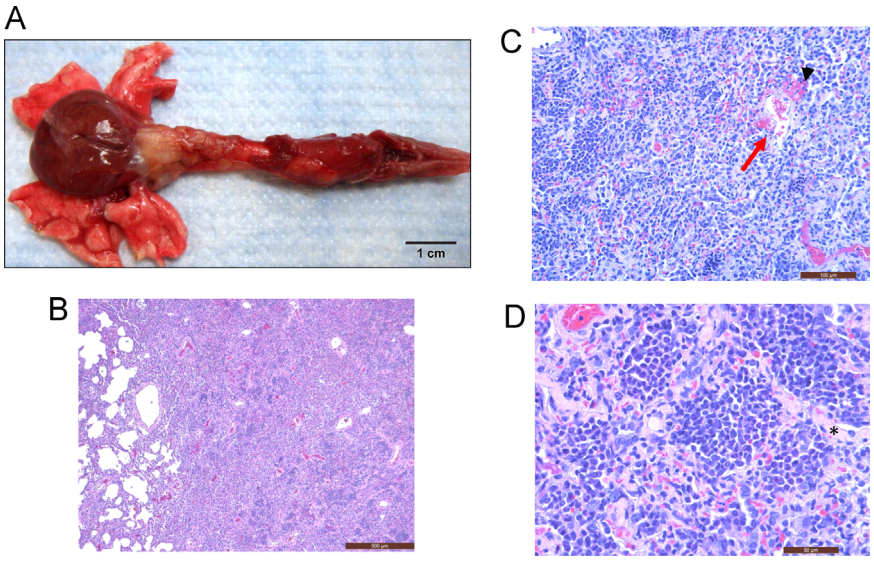

Fig. 6. Gross and Histopathology. (A) Gross lung pathology demonstrating mostly normal lung with multifocal to coalescing moderate interstitial pneumonia in the left caudal lung lobe. (B) Low magnification of lung field from MERS-CoV EMC inoculated subject demonstrating pneumonia. (C) High magnification of lung field from a MERS-CoV-EMC-inoculated subject with evidence of pneumonia; interstitial lymphohistiocytic neutrophilic with type II pneumocyte hyperplasia (red arrow), and extramedullary hematopoiesis (Black arrow). (D) High magnification of a lung field from a MERS-CoV EMC infected subject demonstrating pneumonia with interstitial, neutrophilic with type II pneymocyte hyperplasia and fibrosis (*).

sequences against either MERS-JOR or MERS-EMC spike reference sequences obtained from GenBank (MERS-JOR: KC776174, MERS-EMC: JX869059). To generate a comparison between study stocks and references, spike sequences obtained from sequencing and associated reference sequences were aligned using Clustal Omega with default settings (Goujon et al., 2010; McWilliam et al., 2013; Sievers et al., 2011). The resulting clustal alignment was filtered for alignment positions with at least one variant base using a custom Python script. Potential coding changes were assessed by BLASTX alignments (Altschul et al., 1990).

Challenge and monitoring of NHPs

Ten common marmosets, ranging in weight from 250 g to 475 g and age from 3 to 9 years were divided into 4 groups. Mock inoculated subjects ($n=2$) received DMEM supplemented with 5% FBS by IT inoculation. Two subjects received inactivated virus by IT inoculation; one subject received inactivated MERS-JOR virus isolate, and one subject received inactivated MERS-EMC virus isolate. Three marmosets received 5×10^7 PFU of MERS-JOR and 3 others received 5×10^7 PFU of MERS-EMC by IT inoculation. Prior to handling, marmosets were anesthetized with isoflurane to effect. IT inoculation was performed by placement of a 20 gauge $\times$ 1 in. catheter into the trachea followed by installation of the virus inoculum in a 0.2 mL volume followed by a 0.2 mL air flush of the syringe and catheter. All animal procedures were approved by the National Institute of Allergy and Infectious Diseases (NIAID) Animal Care and Use Committee, and adhered to National Institutes of Health (NIH) policies. The experiments were carried out at the NIAID Integrated Research Facility, an AAALAC and AALAS accredited facility.

Prior to and after inoculation, CT scans, physical exams, including temperature and weight measurements were performed, oropharyngeal and rectal swabs, and stool samples were collected (Fig. 2). NHPs were monitored at least twice daily. A pre-established scale was used to evaluate subject health and disease progression. These criteria included: (1) overall clinical appearance, (2) labored breathing, (3) activity and behavior, (4), responsiveness, and (5) core body temperatures. No subjects met moribund clinical endpoint criteria by study end. Eight of 10 marmosets were humanely euthanized for histopathological and virological analysis. Blood withdrawal was performed pre-inoculation, either day 4 or 5 post-inoculation, and at necropsy.

Table 2
MERS-CoV Spike primers for amplification and sequencing.

Primer name	Sequence	Location relative to Spike AUG start codon
Fw 1 MERS SPIKE	GTAATATCTCTCCTGTCGCAG	−43
Rv 2 MERS SPIKE	GCTCTGCGTATATAACCATCAAC	194
Fw 2 MERS SPIKE	GTATGTTGATTTGTACGGCG	1007
Rv 3 MERS SPIKE	CGCAATTGCCTAATTGAGAG	807
Fw 3 MERS SPIKE	CATGACTGAGCAATTACAGATG	1810
Rv 4 MERS SPIKE	CTGCCAGTAGATATAGAAACAGG	1686
Fw 4 MERS SPIKE	CCAGGATGATTCTGTACG	2648
Rv 5 MERS SPIKE	CTATATGTGTGCCTTGACCG	2523
Fw 5 MERS SPIKE	CAACGTCTTGATGTTCTCG	3370
Rv 6 MERS SPIKE	GCAGTGACCAAAAGAGAG	3166

Computed tomography and image analysis

We acquired high resolution chest CT scans, without contrast, using a hybrid Philips Gemini 16 slice PET/CT scanner specifically designed to function in a Biological Safety Level 4 environment. Due to the rapid respiratory rate of marmosets, a breath hold could not be performed. The CT parameters were as follows: helical scan, 140 kVp, 300 mA s, 90 mm field of view, 0.5 mm/rotation table speed, high-resolution collimation of 16×0.75 mm^2, 0.8 mm slice thickness, and 0.4 mm increment covering the whole lung. The images were acquired using a standard algorithm and reconstructed using a Y-detail algorithm. Images were analyzed as

previously described (Via et al., 2013). Unpaired *t*-test of peak abnormal lung volume was performed with Graphpad Prism 6.0 (GraphPad Software, CA, USA).

Hematology and serology

Complete blood cell differential count was determined from blood samples collected in EDTA-coated blood tubes and analyzed using a Sysmex XT2000V™ hematology analyzer (Sysmex America).

Quantification of viremia by quantitative RT-PCR

Viral load in samples was determined by quantitative PCR using the following primer probe set: forward primer: 5′TGGCC GTGGTGGTTATCACT 3′, reverse primer: 5′CTCAAAATCGTCCATCCA CTCA3′, and probe 5′6-FAM/CACCCCATTCCACTATGAGCGAGACAAC/ 36-TAMSp/3′. Cycling conditions were 48 °C for 30 min and 95 °C for 10 min for the RT-step followed by 95 °C for 15 s and 60 °C for 60 s for 40 cycles. The TaqMan One-Step RT-PCR Master Mix was used (Life Technologies, NY, USA). Samples were extracted with Trizol and screened for the presence of MERS-CoV using specific primers on an Applied Biosystems 7900HT fast real time PCR system (Life Technologies). The limit of detection was 100 gene copies.

Plaque assay and $FRNA_{50}$

Virus stock and tissue samples were excised at necropsy, flash frozen, and stored at −80 °C. For tissues, a w/v homogenate between 10% and 30% was generated. Serial 10-fold dilutions were made for virus stocks, growth curve samples, and tissues and incubated on confluent VeroE6 cells using 0.8% tragacanth in EMEM 2% FBS, and 1% PS overlay and incubated for 5 days. Following incubation, tragacanth overlays were removed, the monolayers were stained with crystal violet (0.1% crystal violet, 20% ethanol 10% formalin v/v), and plaques were enumerated.

Serum samples taken at necropsy or experiment end were heat inactivated at 56 °C for 1 h then serial diluted and mixed with 120 PFU (final MOI=1.0) of either MERS-JOR or MERS-EMC and incubated for 1 h. After incubation virus and serum mixture was added to VeroE6 cells (ATCC, Manassas VA) for 1 h at 37 °C, 5% CO_2 on 96 well Operetta (Perkin-Elmer) compatible plates. Negative control (no virus and no serum) samples and positive control (virus+rabbit polyclonal antibody to the MERS Spike protein (Sino Biological)) samples were also included. Cells were washed and incubated for 24 h followed by fixation with 20% NBF. MERS-CoV infection was visualized by fluorescence using a MERS-CoV anti-Spike antibody (Sino Biological) on an Operetta High Content Imager (Perkin-Elmer). The dilution at which 50% inhibition of relative fluorescence intensity was observed was reported as the $FRNA_{50}$.

Histopathology and immunohistochemistry

Forty-one tissues from all major organ systems were collected and fixed in 10% neutral buffered formalin (NBF) for 30 days. Following fixation in 10% NBF tissues were processed following standard procedures. Hematoxylin and eosin (HE) stain was applied using the Leica automated staining system (Leica, Microsystems). Stained slides were then examined via standard light microscopy. To detect MERS-CoV antigen, IHC was performed using a rabbit polyclonal antiserum against MERS-CoV (Sino Biological P.R. China) (1:1000). Tissues from an uninfected control animal were used to validate all IHC procedures. HE and IHC sections were examined by light microscopy by the veterinary pathologists (SY and LH).

Author summary

In this experiment, we sought to determine if there were virus specific differences in disease progression following intratracheal inoculation of common marmosets with Middle Eastern Respiratory Syndrome Coronavirus, commonly known as MERS-CoV, with two common laboratory viral isolates (MERS-EMC and MERS-Jordan). In contrast to previous results, we observed a non-lethal disease and few, if any, signs of virus-specific pathology. In addition, we were unable to isolate infectious virus from tissues. Computed tomography was used to evaluate disease progression and provide quantitative data for comparisons between mock-exposed, inactivated virus-exposed, and virus-exposed subjects. The data indicate that marmosets do not faithfully replicate human MERS pathogenesis and that alternate models must be developed to efficacy test medical countermeasures.

Acknowledgments

This work was supported by the National Institute of Allergy and Infectious Disease, Division of Intramural Research. We are grateful to Marisa St. Claire, Russell Byrum, Dan Ragland, and the entire EVPS and IRF team for their contributions to these studies. We thank Jiro Wada for his contribution to the preparation of figures and Laura Bollinger for providing technical writing services for preparation of this manuscript. The content of this publication does not necessarily reflect the views or policies of the US Department of Health and Human Services (DHHS) or of the institutions and companies affiliated with the authors. This work was funded in part through Battelle Memorial Institute's prime contract with the US National Institute of Allergy and Infectious Diseases (NIAID) under Contract no. HHSN272200700016I. B.L.O., M.R.H., J.C.J. performed this work as employees of Battelle Memorial Institute. Subcontractors to Battelle Memorial Institute who performed this work are E.P. an employee of Tunnell Government Services, Inc.; N. O., S.Y. and L.H. are employees of Charles River Laboratories, S.M. an employee of MRI Global, CB an employee of MedRelief.

References

Altschul, S.F., Gish, W., Miller, W., Myers, E.W., Lipman, D.J., 1990. Basic local alignment search tool. J. Mol. Biol. 215, 403–410.

Arabi, Y.M., Arifi, A.A., Balkhy, H.H., Najm, H., Aldawood, A.S., Ghabashi, A., Hawa, H., Alothman, A., Khaldi, A., Al Raiy, B., 2014. Clinical course and outcomes of critically ill patients with Middle East respiratory syndrome coronavirus infection. Ann. Intern. Med. 160, 389–397.

Assiri, A., Al-Tawfiq, J.A., Al-Rabeeah, A.A., Al-Rabiah, F.A., Al-Hajjar, S., Al-Barrak, A., Flemban, H., Al-Nassir, W.N., Balkhy, H.H., Al-Hakeem, R.F., Makhdoom, H.Q., Zumla, A.I., Memish, Z.A., 2013. Epidemiological, demographic, and clinical characteristics of 47 cases of Middle East respiratory syndrome coronavirus disease from Saudi Arabia: a descriptive study. Lancet Infect. Dis. 13, 752–761.

Channappanavar, R., Fett, C., Zhao, J., Meyerholz, D.K., Perlman, S., 2014a. Virus-specific memory CD8 T cells provide substantial protection from lethal severe acute respiratory syndrome coronavirus infection. J. Virol. 88, 11034–11044.

Channappanavar, R., Zhao, J., Perlman, S., 2014b. T cell-mediated immune response to respiratory coronaviruses. Immunol. Res. 59, 118–128.

Coleman, C.M., Matthews, K.L., Goicochea, L., Frieman, M.B., 2014. Wild-type and innate immune-deficient mice are not susceptible to the Middle East respiratory syndrome coronavirus. J. Gen. Virol. 95, 408–412.

Cotten, M., Lam, T.T., Watson, S.J., Palser, A.L., Petrova, V., Grant, P., Pybus, O.G., Rambaut, A., Guan, Y., Pillay, D., Kellam, P., Nastouli, E., 2013. Full-genome deep sequencing and phylogenetic analysis of novel human betacoronavirus. Emerg. Infect. Dis. 19, 736–742b.

de Wit, E., Rasmussen, A.L., Falzarano, D., Bushmaker, T., Feldmann, F., Brining, D.L., Fischer, E.R., Martellaro, C., Okumura, A., Chang, J., Scott, D., Benecke, A.G., Katze, M.G., Feldmann, H., Munster, V.J., 2013. Middle East respiratory syndrome coronavirus (MERS-CoV) causes transient lower respiratory tract infection in rhesus macaques. Proc. Natl. Acad. Sci. USA 110, 16598–16603.

Dyall, J., Johnson, R.F., Chen, D.Y., Huzella, L., Ragland, D.R., Mollura, D.J., Byrum, R., Reba, R.C., Jennings, G., Jahrling, P.B., Blaney, J.E., Paragas, J., 2011. Evaluation of monkeypox disease progression by molecular imaging. J. Infect. Dis. 204, 1902–1911.

Elke, G., Fuld, M.K., Halaweish, A.F., Grychtol, B., Weiler, N., Hoffman, E.A., Frerichs, I., 2013. Quantification of ventilation distribution in regional lung injury by electrical impedance tomography and xenon computed tomography. Physiol. Meas. 34, 1303–1318.

Falzarano, D., de Wit, E., Feldmann, F., Rasmussen, A.L., Okumura, A., Peng, X., Thomas, M.J., van Doremalen, N., Haddock, E., Nagy, L., LaCasse, R., Liu, T., Zhu, J., McLellan, J.S., Scott, D.P., Katze, M.G., Feldmann, H., Munster, V.J., 2014. Infection with MERS-CoV causes lethal pneumonia in the common marmoset. PLoS Pathog. 10, e1004250.

Falzarano, D., de Wit, E., Rasmussen, A.L., Feldmann, F., Okumura, A., Scott, D.P., Brining, D., Bushmaker, T., Martellaro, C., Baseler, L., Benecke, A.G., Katze, M.G., Munster, V.J., Feldmann, H., 2013. Treatment with interferon-alpha2b and ribavirin improves outcome in MERS-CoV-infected rhesus macaques. Nat. Med. 19, 1313–1317.

Frey, K.G., Redden, C.L., Bishop-Lilly, K.A., Johnson, R., Hensley, L.E., Raviprakash, K., Luke, T., Kochel, T., Mokashi, V.P., Defang, GN., 2014. Full-genome sequence of human betacoronavirus 2c Jordan-N3/2012 after serial passage in mammalian cells. Genome Announc. 2 (3), e00324-14. 10.1128/genomeA.00324-14.

Goujon, M., McWilliam, H., Li, W., Valentin, F., Squizzato, S., Paern, J., Lopez, R., 2010. A new bioinformatics analysis tools framework at EMBL-EBI. Nucleic Acids Res. 38, W695–W699.

Jonsson, C.B., Camp, J.V., Wu, A., Zheng, H., Kraenzle, J.L., Biller, A.E., Vanover, C.D., Chu, Y.K., Ng, C.K., Proctor, M., Sherwood, L., Steffen, M.C., Mollura, D.J., 2012. Molecular imaging reveals a progressive pulmonary inflammation in lower airways in ferrets infected with 2009 H1N1 pandemic influenza virus. PLoS One 7, e40094.

Li, M., Jirapatnakul, A., Biancardi, A., Riccio, M.L., Weiss, R.S., Reeves, A.P., 2013. Growth pattern analysis of murine lung neoplasms by advanced semi-automated quantification of micro-CT images. PLoS One 8, e83806.

McWilliam, H., Li, W., Uludag, M., Squizzato, S., Park, Y.M., Buso, N., Cowley, A.P., Lopez, R., 2013. Analysis tool web services from the EMBL-EBI. Nucleic Acids Res. 41, W597–W600.

Romanova, A.L., Nemeth, A.J., Berman, M.D., Guth, J.C., Liotta, E.M., Naidech, A.M., Maas, M.B., 2014. Magnetic resonance imaging versus computed tomography for identification and quantification of intraventricular hemorrhage. J. Stroke Cerebrovasc. Dis.: Off. J. Natl. Stroke Assoc. 23, 2036–2040.

Sievers, F., Wilm, A., Dineen, D., Gibson, T.J., Karplus, K., Li, W., Lopez, R., McWilliam, H., Remmert, M., Soding, J., Thompson, J.D., Higgins, D.G., 2011. Fast, scalable generation of high-quality protein multiple sequence alignments using Clustal Omega. Mol. Syst. Biol. 7, 539.

Via, L.E., Weiner, D.M., Schimel, D., Lin, P.L., Dayao, E., Tankersley, S.L., Cai, Y., Coleman, M.T., Tomko, J., Paripati, P., Orandle, M., Kastenmayer, R.J., Tartakovsky, M., Rosenthal, A., Portevin, D., Eum, S.Y., Lahouar, S., Gagneux, S., Young, D.B., Flynn, J.L., Barry 3rd, C.E., 2013. Differential virulence and disease progression following Mycobacterium tuberculosis complex infection of the common marmoset (*Callithrix jacchus*). Infect. Immun. 81, 2909–2919.

Yao, Y., Bao, L., Deng, W., Xu, L., Li, F., Lv, Q., Yu, P., Chen, T., Xu, Y., Zhu, H., Yuan, J., Gu, S., Wei, Q., Chen, H., Yuen, K.Y., Qin, C., 2014. An animal model of MERS produced by infection of rhesus macaques with MERS coronavirus. J. Infect. Dis. 209, 236–242.

Zaki, A.M., van Boheemen, S., Bestebroer, T.M., Osterhaus, A.D., Fouchier, R.A., 2012. Isolation of a novel coronavirus from a man with pneumonia in Saudi Arabia. N. Engl. J. Med. 367, 1814–1820.

Zhao, J., Li, K., Wohlford-Lenane, C., Agnihothram, S.S., Fett, C., Zhao, J., Gale Jr., M.J., Baric, R.S., Enjuanes, L., Gallagher, T., McCray Jr., P.B., Perlman, S., 2014. Rapid generation of a mouse model for Middle East respiratory syndrome. Proc. Natl. Acad. Sci. USA 111, 4970–4975.